Electronic Supplementary information

Crystalline/Amorphous Hetero-Phase Ru Nanoclusters for Efficient Electrocatalytic Oxygen Reduction and Hydrogen Evolution

Shuangquan Liu[a#], Lanxin Dai[a#], Yunteng Qu[b], Yu Qiu[a], Jianxiong Fan[a], Xue Li[a], Qinghua Zhang[c] and Xiaohui Guo*[a]

[a] Prof. Xiaohui Guo, Dr. Shuangquan Liu, Dr. Yu Qiu, Dr. Jianxiong Fan, Dr. Lanxin Dai, Dr. Xue Li, Key Lab of Synthetic and Natural Functional Molecule Chemistry of Ministry of Education, and the College of Chemistry and Materials Science, Northwest University, Xi'an 710069, P. R. China.

[b] Dr. Yunteng Qu, Department of Chemistry, iChEM, University of Science and Technology of China, Hefei 230026, P. R. China.

[c] Prof. Qinghua Zhang, Beijing National Laboratory for Condensed Matter Physics, Institute of Physics, Chinese Academy of Sciences, Beijing 100190, P. R. China.

#present equally contribute to this work.

*Corresponding Email: guoxh2009@nwu.edu.cn, Tel (Fax): (+)86-29-81535025

DFT calculation:

The calculations were performed using the Vienna ab initio Simulation Package (VASP).[1,2] Perdew-Burke-Ernzerhof (PBE) was used to perform all Spin-polarization density functional theory (DFT) calculations within the generalized gradient approximation (GGA).[3] Projected augmented wave (PAW) potentials was chosen to describe the ionic cores.[4,5] A plane wave basis was set with a kinetic energy cutoff of 400eV taking valence electrons into account. Partial occupancies of the Kohn−Sham orbitals were allowed using the Gaussian smearing method and a width of 0.05 eV. The electronic energy was considered self-consistent when the energy change was smaller than 10^{-6} eV. A geometry optimization was considered convergent when the energy change was smaller than 0.05 eV $Å^{-1}$. In addition, for the Ru atoms, the U schemes need to be applied, and the U has been set as 2.75 eV. The free energy was calculated using the equation:

$$G = E + ZPE - TS$$

where G, E, ZPE and TS are the free energy, total energy from DFT calculations, zero point energy and entropic contributions, respectively.

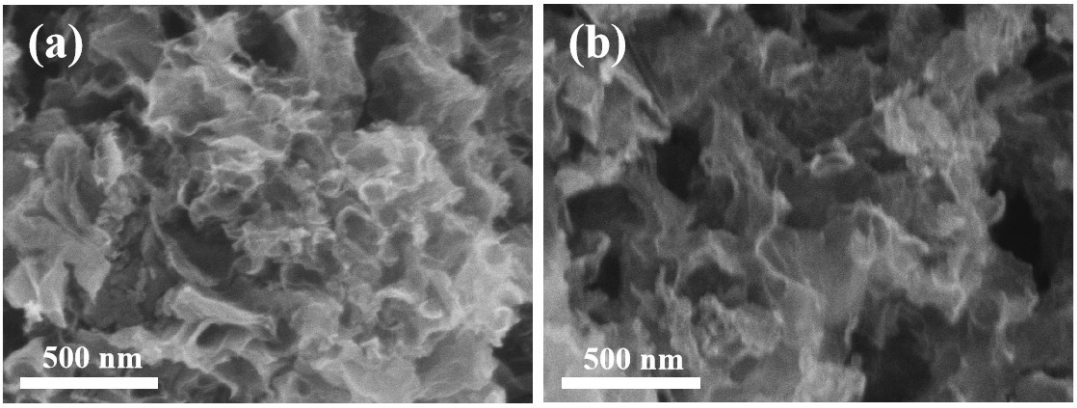

Figure S1. (a-b) SEM image of N-G and Ru/N-G-500, respectively.

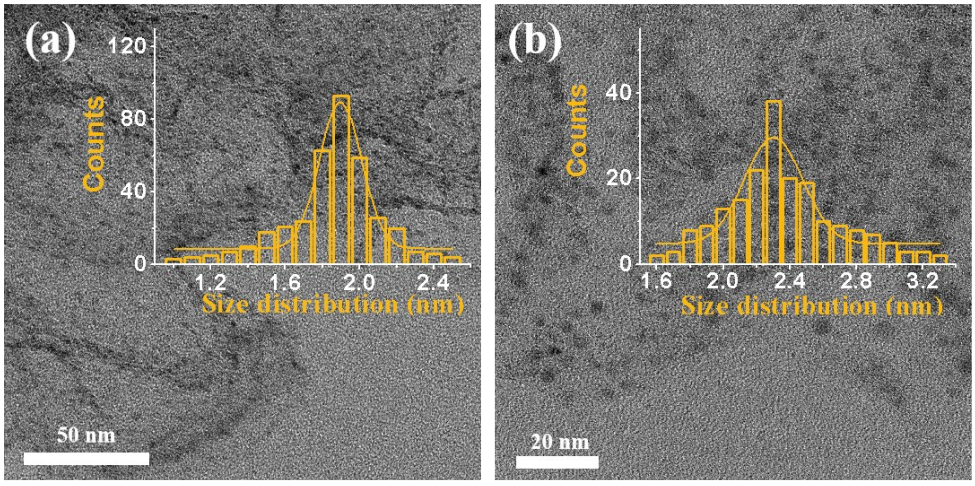

Figure S2. (a) TEM images of Ru/N-G-300, inset shows the corresponding Ru nanoclusters distribution histogram. (b) TEM images of Ru/N-G-700, inset shows the corresponding Ru nanoclusters distribution histogram.

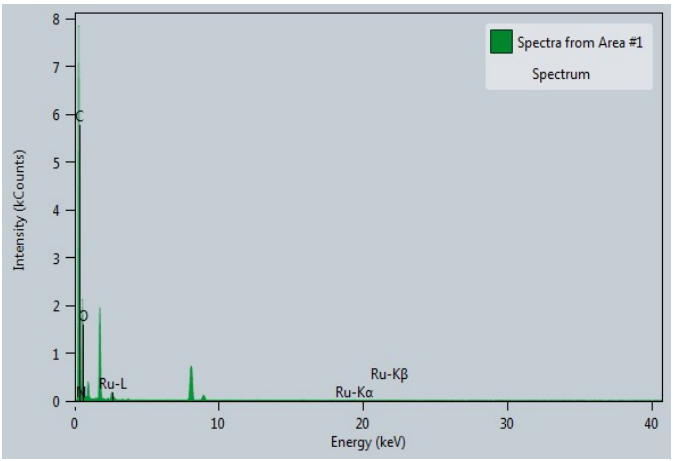

Figure S3. EDX patterns of Ru/N-G-500, the Ru mass fraction is 3.05 %.

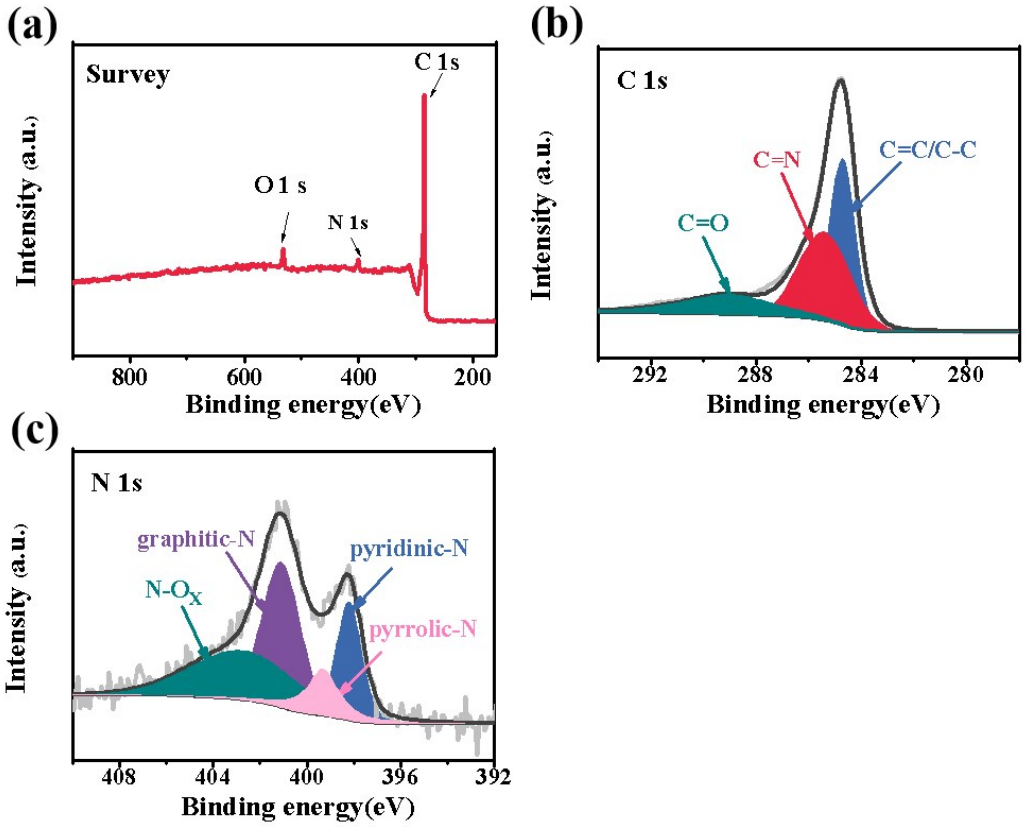

Figure S4. (a) The XPS survey spectrum of the N-G. (b-c) High-resolution of C 1s and N 1s XPS spectra, respectively.

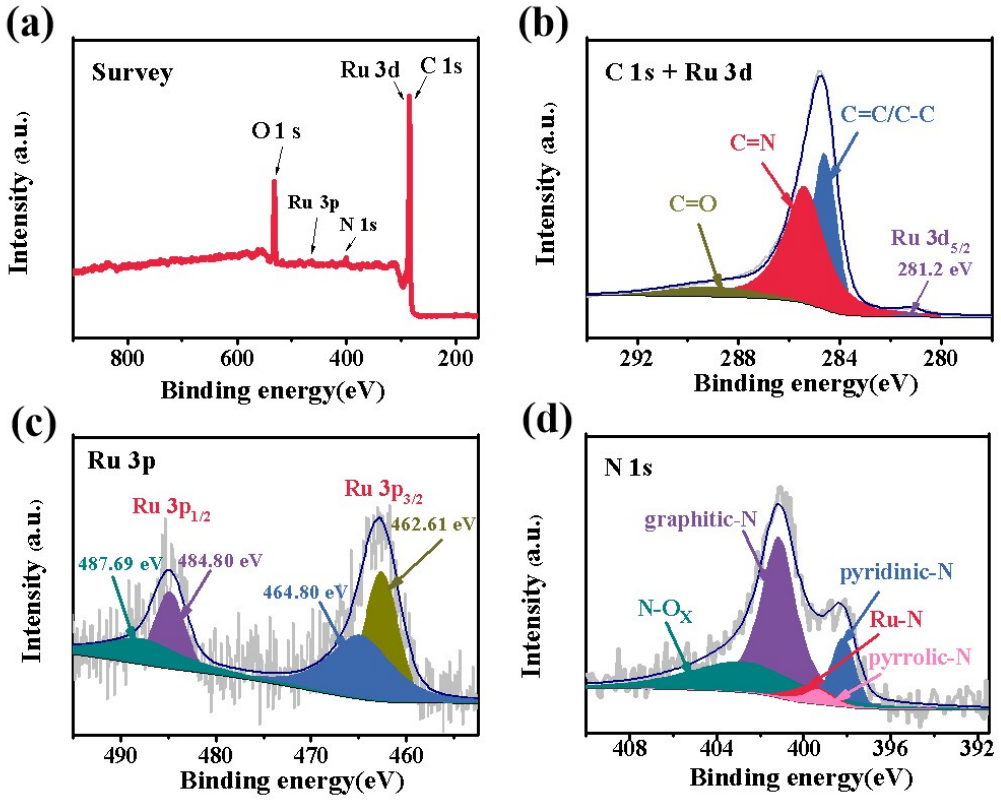

Figure S5. (a) The XPS survey spectrum of the Ru/N-G-300. (b-d) High-resolution of C 1s + Ru 3d, Ru 3p and N 1s XPS spectra, respectively.

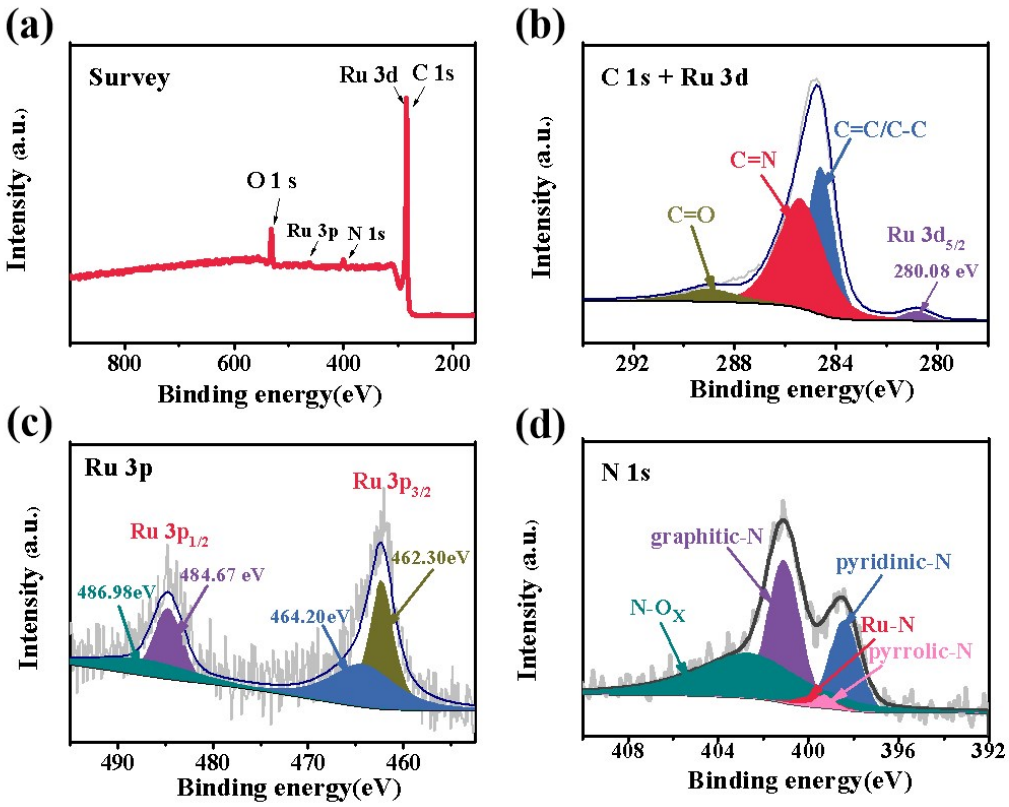

Figure S6. (a) The XPS survey spectrum of the Ru/N-G-700. (b-d) High-resolution of C 1s + Ru 3d, Ru 3p and N 1s XPS spectra, respectively.

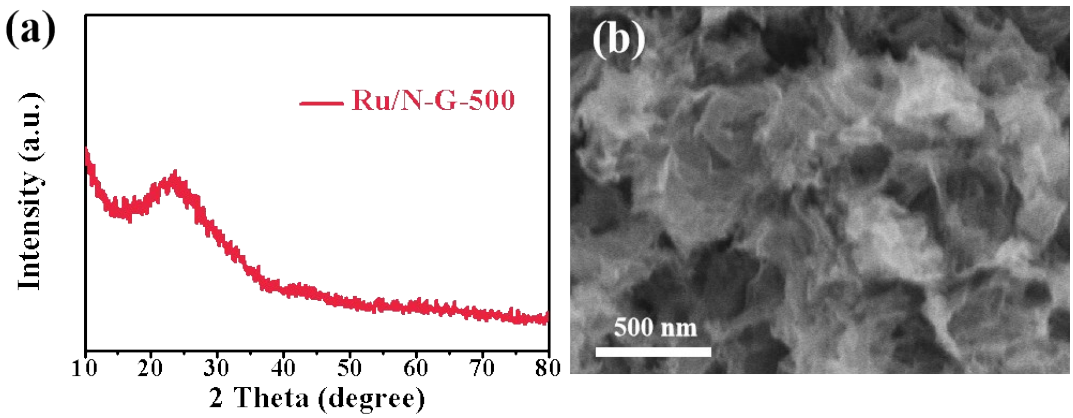

Figure S7. The XRD pattern (a) and SEM image (b) of Ru/N-G-500 after ORR cycles durability test in 0.1 M KOH.

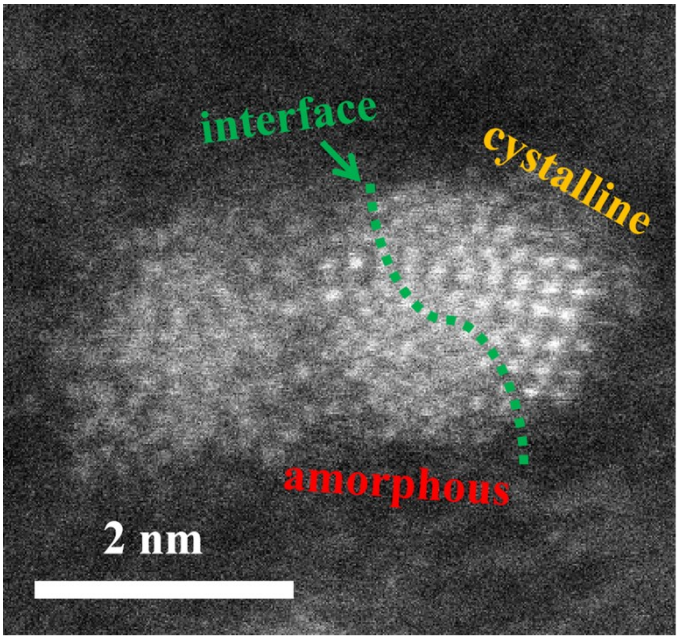

Figure S8. HAADF-STEM images of Ru nanocluster/N-G-500 catalyst after ORR cycles durability test in 0.1 M KOH solution.

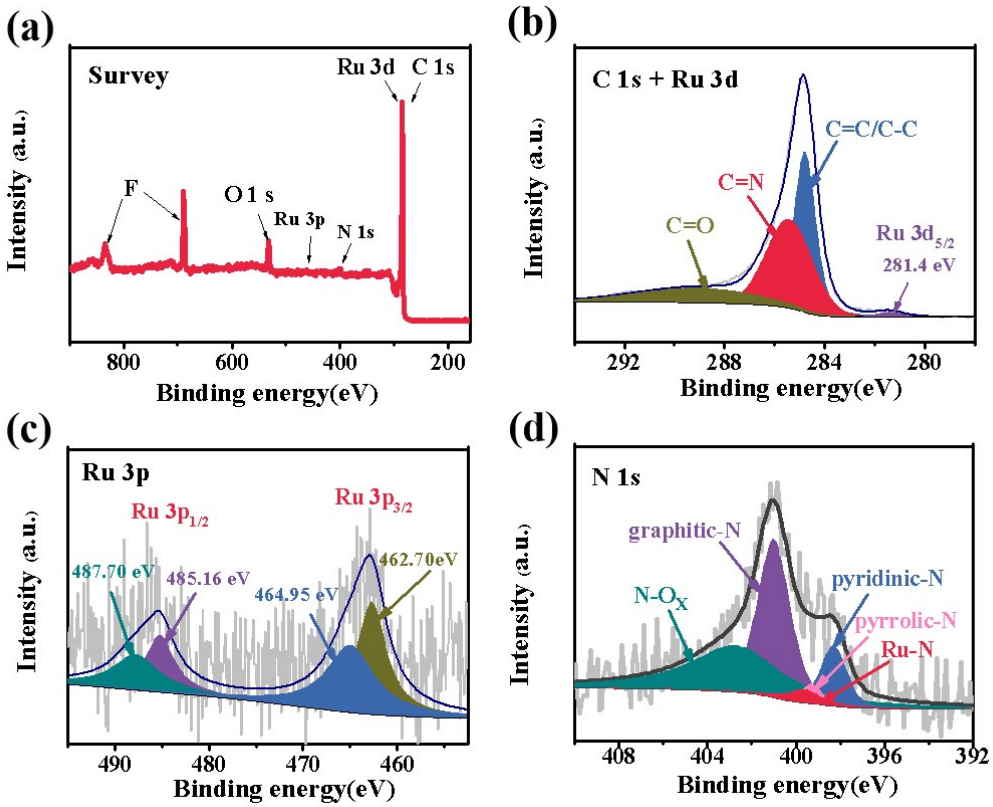

Figure S9. (a) The XPS survey spectrum of the Ru/N-G-500 after ORR cycles durability test in 0.1 M KOH solution. (b-d) High-resolution of C 1s + Ru 3d, Ru 3p and N 1s XPS spectra, respectively.

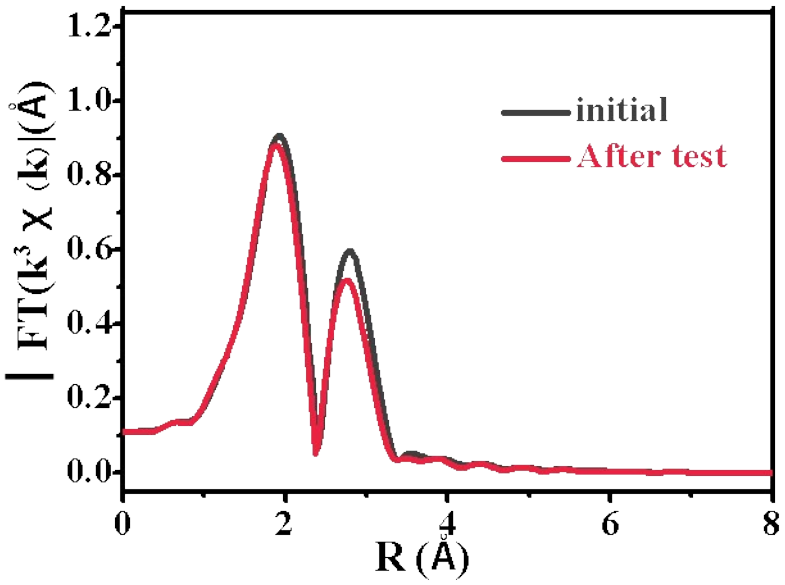

Figure S10. FT-EXAFS spectra of Ru/N-G-500 at the Ru K-edge before and after ORR cycles durability test.

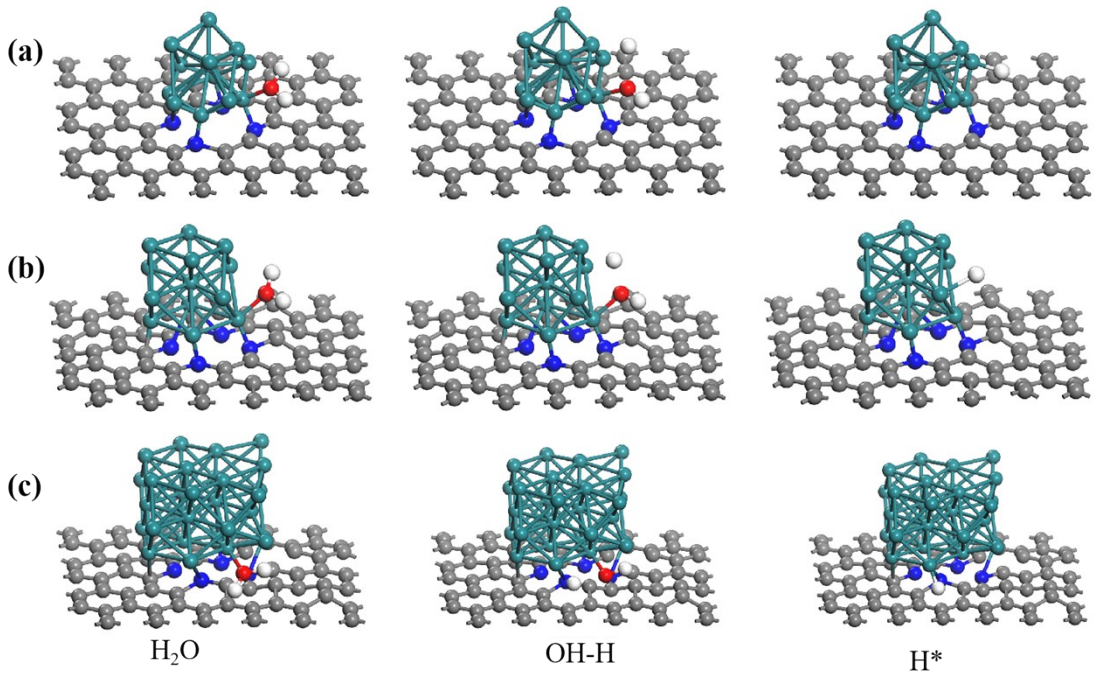

Figure S11. (a-c) The HER chemisorption models of Ru/N-G-300, Ru/N-G-700 and Ru/N-G-500, respectively.

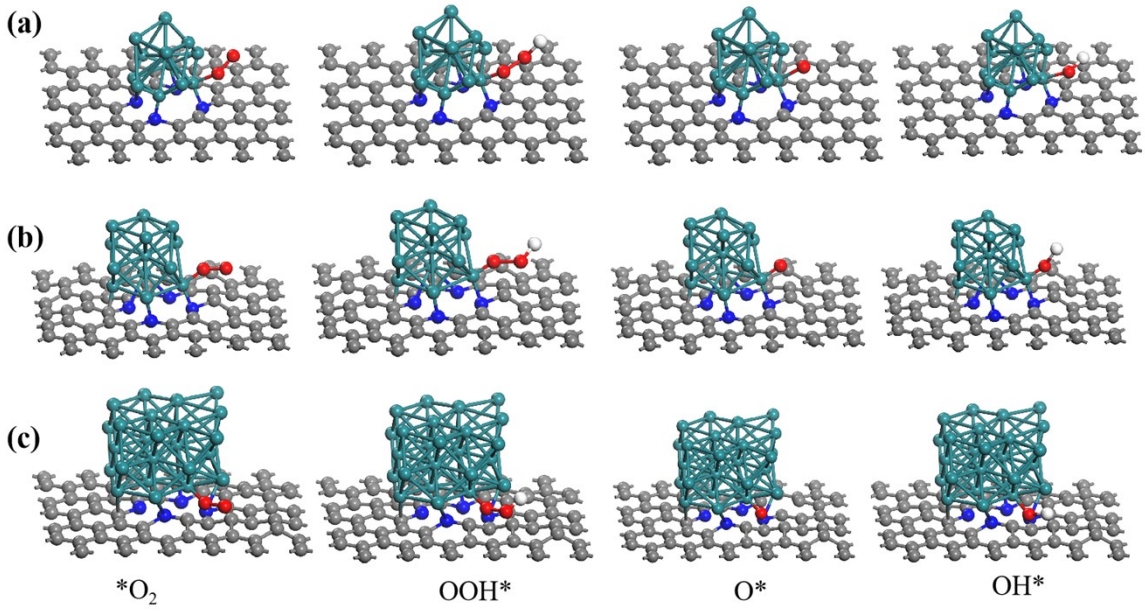

Figure S12. (a-c) The ORR chemisorption models of Ru/N-G-300, Ru/N-G-700 and Ru/N-G-500, respectively.

Table S1. Structural parameters obtained from the curve-fitting analysis of EXAFS spectrum.

Sample	Ru-N		Ru-Ru		σ^2 (Å^2)	ΔE_0 (eV)
	R (Å)	*CN*	*R* (Å)	*CN*		
Ru/N-G-300	2.0130.012	4.1±0.4	2.686±0.016	2.1±0.4	0.0045(O0.0065(Ru)	1.7±1.3
Ru/N-G-500	2.012±0.016	3.9±0.6	2.687±0.016	3.3±0.7		
Ru/N-G-500-After ORR durability test	2.024±0.011	3.9±0.3	2.695±0.011	2.8±0.3		
Ru/N-G-700	2.014±0.022	2.6±0.6	2.675±0.009	5.9±0.5	0.0045(O)0.006(Ru)	

Table S2. Free energy calculated results of Ru/N-G and 20 wt% Pt C surface HER reaction path.

Catalysts	H_2O	OH-H	H*
Ru/N-G-300	0	0.871	0.401
Ru/N-G-500	0	0.564	0.175
Ru/N-G-700	0	1.031	0.583
20 wt% Pt/C	0	0.7922	0.366

Table S3. Free energy calculated results of Ru/N-G and 20 wt% Pt C surface ORR reaction path.

Catalysts		O_2	OOH*	O*	OH^-
Ru/N-G-300	U=0 V	4.92	4.2736	2.7416	1.1455

	U=1.23 V	0	0.5836	0.2816	-0.0845
Ru/N-G-500	U=0 V	4.92	3.795	2.4515	0.851
	U=1.23 V	0	0.105	-0.0085	-0.379
Ru/N-G-700	U=0 V	4.92	4.4115	2.8752	1.2555
	U=1.23 V	0	0.7215	0.4152	0.0255
20 wt% Pt C	U=0 V	4.92	4.127	2.5155	0.9255
	U=1.23 V	0	0.437	0.0555	-0.3045

Table S4. Comparison of HER activity of various Ru-based catalysts in Alkaline solution.

Catalysts	Overpotential @ 10 mA cm^{-2} (mV)	Electrolyte solution	Ru loading on the electrode (mg)	Reference
Ru/N-G-500	20.1	1 M KOH	0.00075	This work
Ru@NGT	60	1 M KOH	0.00708	[6]
0.4-Ru@NG-750	40	1 M KOH	/	[7]
$Pd_{50}Ru_{50}$/CNs	37.3	0.1 M KOH	/	[8]
Pd-Ru@NG	42	1 M KOH	0.011	[9]
Cu_{2-x}@RuNPS	82	1 M KOH	/	[10]
RuCo@NC	28	1 M KOH	0.00069	[11]
$Rh_{50}Ru_{50}$@UiO-66-NH_2	177	1 M KOH	0.00087	[12]
Fe@Ru/NC-9%	55	1 M KOH	0.0014	[13]
Ru/C_3N_4/C	79	0.1 M KOH	/	[14]
RuP_2@NPC	52	1 M KOH	0.016	[15]

Ru-MoO_2	29	1 M KOH	0.0032	[16]
Ru-TiO_2	150	0.1 M KOH	0.0024	[17]
RuPx@NPC	74	1 M KOH	0.0032	[18]
Co-B_i-Ru/Ru/BNC	145	1 M KOH	0.00011	[19]
NiRu@N-C	32	1 M KOH	0.00037	[20]
Au-Ru-2 NWs	50	1 M KOH	/	[21]
Ru@GnP	22	1 M KOH	0.0034	[22]
Ru@CN-0.16	32	1 M KOH	0.0015	[23]
Ru/C	53	1 M KOH	/	[24]
RuNC	38	1 M KOH	/	[25]

Table S5. Comparison of ORR activity of various Ru-based catalysts in O_2-saturated 0.1 M KOH.

Catalysts	Onset potential for ORR (V vs. RHE)	Half-wave potential $E_{1/2}$	Diffusion-limited current density (mA cm^{-2})	Ru loading on the electrode (mg)	Reference
Ru/N-G-500	0.978	0.847	-5.78	0.0025	This work
Ru@NGT	0.97	0.83	-5.0	0.0071	[6]
0.4-Ru@NG-750	0.945	0.826	-	/	[7]
$Pd_{50}Ru_{50}$/CNs	0.903	0.799	-5.14	/	[8]
Ru/CNT	0.76	-	-3.89	0.0002	[26]
Ru/MWCNT	0.894	0.723	-4.7	0.0006	[27]
$Ru_{0.2}Co_{2.8}O_4$	0.88	0.77	-4.41	/	[28]
$RuTe_2$/C	0.96	0.72	-	0.0069	[29]
CoRu-O/A@HNC-2	0.937	0.821	-	0.0002	[30]

$Ru_{0.95}Co_{0.05}$/C	-	0.839	-	/	[31]

References:

1 G. Kresse and J. Furthmüller, Efficiency of Ab-Initio Total Energy Calculations for Metals and Semiconductors Using a Plane-Wave Basis Set，*Comput. Mater. Sci.* 1996, **6**, 15, DOI: 10.1016/0927-0256(96)00008-0.

2 G. Kresse and J. Furthmüller, Efficient Iterative Schemes for Ab Initio Total-Energy Calculations Using a Plane-Wave Basis Set, *Phys. Rev. B*, 1996, **54**, 11169, DOI: 10.1103/PhysRevB.54.11169.

3 J. P. Perdew, K. Burke and M. Ernzerhof, Generalized Gradient Approximation Made Simple, *Phys. Rev. Lett.*, 1996, **77**, 3865, DOI: 10.1103/PhysRevLett.77.3865.

4 G. Kresse and D. Joubert, From Ultrasoft Pseudopotentials to The Projector Augmented-Wave Method, *Phys. Rev. B*, 1999, **59**, 1758, DOI: 10.1103/PhysRevB.59.1758.

5 P. E. Blöchl, Projector Augmented-Wave Method., *Phys. Rev. B*, 1994, **50**, 17953, DOI: 10.1103/PhysRevB.50.17953.

6 B. K. Barman, B. Sarkar, P. Ghosh, M. Ghosh, G. M. Rao and K. K. Nanda, In Situ Decoration of Ultrafine Ru Nanocrystals on N-Doped Graphene Tube and Their Applications as Oxygen Reduction and Hydrogen Evolution Catalyst, *ACS Appl. Energy Mater.*, 2019, **2**, 7330, DOI: 10.1021/acsaem.9b01318.

7 L. Bai, Z. Duan, X. Wen, R. Si, Q. Zhang and J. Guan, Highly Dispersed

Ruthenium-Based Multifunctional Electrocatalyst, *ACS Catal.*, 2019, **9**, 9897-9904, DOI: 10.1021/acscatal.9b03514.

8 J. Tian, W. Wu, Z. Tang, Y. Wu, R. Burns, B. Tichnell, Z. Liu and S. Chen, Oxygen Reduction Reaction and Hydrogen Evolution Reaction Catalyzed by Pd–Ru Nanoparticles Encapsulated in Porous Carbon Nanosheets, *Catalysts*, 2018, **8**, 329, DOI: 10.3390/catal8080329.

9 B. K. Barman, B. Sarkar and K. K. Nanda, Pd-Coated Ru Nanocrystals Supported on N-Doped Graphene as HER and ORR Electrocatalysts, *Chem. Commun.,* 2019, **55**, 13928-13931, DOI: 10.1039/C9CC06208D.

10 D. Yoon, J. Lee, B. Seo, B. Kim, H. Baik, S. H. Joo and K. Lee, Cactus-Like Hollow $Cu_{2-x}S$@Ru Nanoplates as Excellent and Robust Electrocatalysts for the Alkaline Hydrogen Evolution Reaction, *Small*, 2017, **13**, 1700052, DOI: 10.1002/smll.201700052.

11 J. Su, Y. Yang, G. Xia, J. Chen, P. Jiang and Q. Chen, Ruthenium-Cobalt Nanoalloys Encapsulated in Nitrogen-Doped Graphene as Active Electrocatalysts for Producing Hydrogen in Alkaline Media, *Nat. Commun.*, 2017, **8**, 14969, DOI: 10.1038/ncomms14969.

12 Z. Ding, K. Wang, Z. Mai, G. He, Z. Liu and Z. Tang, RhRu Alloyed Nanoparticles Confined within Metal Organic Frameworks for Electrochemical Hydrogen Evolution at All pH Values, *Int. J. Hydrogen Energy*, 2019, **44**, 24680-24689, DOI: 10.1016/j.ijhydene.2019.07.244.

13 Z. Zong, Z. Qian, Z. Tang, Z. Liu, Y. Tian and S. Wang, Hydrogen Evolution and Oxygen Reduction Reactions Catalyzed by Core-Shelled Fe@Ru Nanoparticles Embedded in Porous Dodecahedron Carbon, *J. Alloys Compd.*, 2019, **784**, 447-455, DOI: 10.1016/j.jallcom.2019.01.088.

14 Y. Zheng, Y. Jiao, Y. Zhu , L. Li , Y. Han, Y. Chen, M. Jaroniec and S. Qiao, High Electrocatalytic Hydrogen Evolution Activity of An Anomalous Ruthenium Catalyst, *J. Am. Chem. Soc*, 2016, **138**, 16174-16181, DOI: 10.1021/jacs.6b11291.

15 Z. Pu, I. Amiinu, Z. Kou, W. Li and S. Mu, RuP_2-Based Catalysts with Platinum-Like Activity and Higher Durability for the Hydrogen Evolution Reaction at All pH Values, *Angew. Chem. Int. Ed.*, 2017, **56**, 11559-11564, DOI: 10.1002/anie.201704911.

16 P. Jiang, Y. Yang, R. Shi, G. Xia, J. Chen, J. Su and Q. Chen, Pt-Like Electrocatalytic Behavior of Ru–MoO_2 Nanocomposites for the Hydrogen Evolution Reaction, *J. Mater. Chem. A*, 2017, **5**, 5475-5485, DOI: 10.1039/C6TA09994G.

17 S. Nong, W. Dong, J. Yin, B. Dong, Y. Lu, X. Yuan, X. Wang, K. Bu, M. Chen, S. Jiang, L. Liu**,** M. Sui and F. Huang, Well-Dispersed Ruthenium in Mesoporous Crystal TiO_2 as an Advanced Electrocatalyst for Hydrogen Evolution Reaction, *J. Am. Chem. Soc.*, 2018, **140**, 5719, DOI: 10.1021/jacs.7b13736.

18 J. Chi, W. Gao, J. Lin, B. Dong, K. Yan, J. Qin, B. Liu, Y. Chai and C. Liu, Hydrogen Evolution Activity of Ruthenium Phosphides Encapsulated in Nitrogen and

Phosphorous-Codoped Hollow Carbon Nanospheres, *ChemSusChem*, 2018**, 11**, 743-752, DOI: 10.1002/cssc.201702010.

19 Q. Hu, G. Li, Z. Han, Z. Wang, X. Huang, X. Chai, Q. Zhang, J. Liu and C. He, General Synthesis of Ultrathin Metal Borate Nanomeshes Enabled by 3D Bark-Like N-Doped Carbon for Electrocatalysis, *Adv. Energy Mater.,* 2019, **9**, 1970109, DOI: 10.1002/aenm.201901130.

20 Y. Xu, S. Yin, C. Li, K. Deng, H. Xue, X. Li, H. Wang and L. Wang, Low-Ruthenium-Content NiRu Nanoalloys Encapsulated in Nitrogen-Doped Carbon as Highly Efficient and pH-Universal Electrocatalysts for the Hydrogen Evolution Reaction, *J. Mater. Chem. A*, 2018, **6**, 1376-1381, DOI: 10.1039/C7TA09939H.

21 Q. Lu, A. Wang, Y. Gong, W. Hao, H. Cheng, J. Chen, B. Li, N. Yang, W. Niu, J. Wang, Y. Yu, X. Zhang, Y. Chen, Z. Fan, X. Wu, J. Chen, J. Luo, S. Li, L. Gu and H. Zhang, Crystal Phase-Based Epitaxial Growth of Hybrid Noble Metal Nanostructures on 4H/fcc Au Nanowires, *Nat. Chem.*, 2018, **10**, 456-461, DOI: 10.1038/s41557-018-0012-0.

22 F. Li, G. Han, H-J. Noh, I. Ahmad, I. Y. Jeon and J-B. Baek, Mechanochemically Assisted Synthesis of A Ru Catalyst for Hydrogen Evolution with Performance Superior to Pt in Both Acidic and Alkaline Media, *Adv. Mater.,* 2018, **30**, 1803676, DOI: 10.1002/adma.201803676.

23 J. Wang, Z. Wei, S. Mao, H. Li and Y. Wang, Highly Uniform Ru Nanoparticles over N-Doped Carbon: pH and Temperature-Universal Hydrogen Release from Water

Reduction, *Energy Environ. Sci.*, 2018, **11**, 800-806, DOI: 10.1039/C7EE03345A.

24 Y. Li, J. Abbott, Y. Sun, J. Sun, Y. Du, X. Han, G. Wu and P. Xu, Ru Nanoassembly Catalysts for Hydrogen Evolution and Oxidation Reactions in Electrolytes at Various pH Values, *Appl. Catal., B*, 2019, **258**, 117952, DOI: 10.1016/j.apcatb.2019.117952.

25 Y. Xiao, W. Liu, Z. Zhang and J. Liu, Controllable Synthesis for Highly Dispersed Ruthenium Clusters Confined in Nitrogen Doped Carbon for Efficient Hydrogen Evolution, *J. Colloid Interface Sci.*, 2020, **571**, 205-212, DOI: 10.1016/j.jcis.2020.03.048.

26 D. M. Fernandes, M. Rocha, C. R. Cárcamo, P. Serp and C. Freire, Ru Single Atoms and Nanoparticles on Carbon Nanotubes as Multifunctional Catalysts, *Dalton Trans.*, 2020*,* **49***,* 10250-10260*,* DOI: 10.1039/D0DT02096F.

27 C. Liu, G. Bai, Z. Jiao, B. Lv, Y. Wang, X. Tong and N. Yang, Particle Size-Control Enables Extraordinary Activity of Ruthenium Nanoparticles/Multiwalled Carbon Nanotube Catalysts Towards the Oxygen Reduction Reaction, *Nanoscale*, 2019**, 11**, 13968-13976, DOI: 10.1039/C9NR05202J.

28 M. Wei, S. Huang, Y. Wang, Y. Liu, Y. He, C. Wang and L. Yang, Nanostructured Ru-Doped Co_3O_4 as An Efficient Electrocatalyst for Oxygen Reduction Reaction in Alkaline Medium, *J. Alloys Compd.*, 2020, **827**, 154207, DOI: 10.1016/j.jallcom.2020.154207.

29 Q. Gong, J. Zheng, Y. Wang, S. Gong, W. Yang, X. Cheng and H. Li, Highly

Stable and Methanol Tolerant $RuTe_2$/C Electrocatalysts for Fuel Cell Applications, *J. Electrochem. Soc.*, 2018, **165**, F876-F882, DOI: 10.1149/2.1291810jes.

30 G. Li, K. Zheng, W. Li, Y. He and C. Xu, Ultralow Ru-Induced Bimetal Electrocatalysts with a Ru-Enriched and Mixed-Valence Surface Anchored on a Hollow Carbon Matrix for Oxygen Reduction and Water Splitting, *ACS Appl. Mater. Interfaces*, 2020, **12**, 51437-51447, DOI: 10.1021/acsami.0c14521.

31 H. Wang, Y. Yang, F. J. DiSalvo, H. D. Abrun, Multifunctional Electrocatalysts: Ru-M (M = Co, Ni, Fe) for Alkaline Fuel Cells and Electrolyzers, *ACS Catal.*, 2020, **10**, 4608-4616，DOI: 10.1021/acscatal.9b05621.